

Quantum-rod dispersed photopolymers for multi-dimensional photonic applications

Xiangping Li,¹ James W. M. Chon,¹ Richard A. Evans,² and Min Gu,^{1,*}

¹ Centre for Micro-Photonics, Faculty of Engineering and Industrial Sciences, Swinburne University of Technology, Hawthorn, Victoria 3122, Australia

² CSIRO Molecular and Health Technologies, Bag 10, Clayton South, Victoria 3169, Australia

*Corresponding author: mgu@swin.edu.au

Abstract: Nanocrystal quantum rods (QRs) have been identified as an important potential key to future photonic devices because of their unique two-photon (2P) excitation, large 2P absorption cross section and polarization sensitivity. 2P excitation in a conventional solid photosensitive medium has driven all-optical devices towards three-dimensional (3D) platform architectures such as 3D photonic crystals, optical circuits and optical memory. The development of a QR-sensitized medium should allow for a polarization-dependent change in refractive index. Such a localized polarization control inside the focus can confine the light not only in 3D but also in additional polarization domain. Here we report on the first 2P absorption excitation of QR-dispersed photopolymers and its application to the fabrication of polarization switched waveguides, multi-dimensional optical patterning and optical memory. This fabrication was achieved by a 2P excited energy transfer process between QRs and azo dyes which facilitated 3D localized polarization sensitivity resulting in the control of light in four dimensions.

©2009 Optical Society of America

OCIS codes: (210.1635) Coding for optical storage; (210.4680) Optical memories, (210.4810) Optical storage-recording materials.

References and links

1. S. Noda, M. Fujita, and T. Asano, "Spontaneous-emission control by photonic crystals and nanocavities," *Nat. Photonics* **1**, 449-458 (2007).
2. K. Minoshima, A. M. Kowalevicz, I. Hartl, E. P. Ippen, and J. G. Fujimoto, "Photonic device fabrication in glass by use of nonlinear materials processing with a femtosecond laser oscillator," *Opt. Lett.* **26**, 1516-1518 (2001).
3. D. A. Parthenopoulos, and P. M. Rentzepis, "Three-dimensional optical storage memory," *Science* **245**, 843-845 (1989).
4. B. H. Cumpston, S. P. Ananthavel, S. Barlow, D. L. Dyer, J. E. Ehrlich, L. L. Erskine, A. A. Heikal, S. M. Kuebler, I.-Y. S. Lee, D. McCord-Maughon, J. Qin, H. Rockel, M. Rumi, X.-L. Wu, S. R. Marder, and J. W. Perry, "Two-photon polymerization initiators for three-dimensional optical data storage and microfabrication," *Nature* **398**, 51-54 (1999).
5. E. Walker, and P. M. Rentzepis, "Two-photon technology: a new dimension," *Nat. Photonics* **2**, 406 - 408 (2008).
6. J. Serbin, and M. Gu, "Experimental evidence for superprism effects in three-dimensional polymer photonic crystals," *Adv. Mater.* **18**, 221-224 (2006).
7. S. Kawata, H.-B. Sun, T. Tanaka, and K. Takada, "Finer features for functional microdevices," *Nature* **412**, 697-698 (2001).
8. H. Ishitobi, Z. Sekkat, and S. Kawata, "Photo-orientation by multiphoton photoselection," *J. Opt. Soc. Am. B* **23**, 868-873 (2006).
9. X. Li, J. W. M. Chon, S. Wu, R. A. Evans, and M. Gu, "Rewritable polarization-encoded multilayer data storage in 2,5-dimethyl-4-(p-nitrophenylazo)anisole doped polymer," *Opt. Lett.* **32**, 277-279 (2007).
10. E. Rothenberg, Y. Ebenstein, M. Kazes, and U. Banin, "Two-photon fluorescence microscopy of single semiconductor quantum rods: Direct observation of highly polarized nonlinear absorption dipole," *J. Phys. Chem. B* **108**, 2797-2800 (2004).
11. K.-T. Yong, J. Qian, I. Roy, H. H. Lee, E. J. Bergey, K. M. Tramposch, S. He, M. T. Swihart, A. Maitra, and P. N. Prasad, "Quantum rod bioconjugates as targeted probes for confocal and two-photon fluorescence imaging of cancer cells," *Nano. Lett.* **7**, 761-765 (2007).
12. A. P. Alivisatos, "Semiconductor clusters, nanocrystals, and quantum dots," *Science* **271**, 933-937 (1996).

13. X. Peng, L. Manna, W. Yang, J. Wickham, E. Scher, A. Kadavanich, and A. P. Alivisatos, "Shape control of CdSe nanocrystals," *Nature* **404**, 59-61 (2000).
 14. X. Li, J. Van Embden, J. W. M. Chon, and M. Gu, "Enhanced two-photon absorption of CdS nanocrystal rods," to be submitted.
 15. J. Hu, L.-S. Li, W. Yang, L. Manna, L.-W. Wang, and A. P. Alivisatos, "Linearly polarized emission from colloidal semiconductor quantum rods," *Science* **292**, 2060-2063 (2001).
 16. L. De Boni, J. J. Rodrigues Jr., D. S. Dos Santos Jr., C. H. T. P. Silva, D. T. Balogh, O. N. Oliveira Jr., S. C. Zilio, L. Misoguti, and C. R. Mendonca, "Two-photon absorption in azoaromatic compounds," *Chem. Phys. Lett.* **361**, 209-213 (2002).
 17. Z. Sekkat, J. Wood, E. F. Aust, W. Knoll, W. Volksen, and R. D. Miller, "Light-induced orientation in a high glass transition temperature polyimide with polar azo dyes in the side chain," *J. Opt. Soc. Am. B* **13**, 1713-1724 (1996).
 18. F. Shieh, A. E. Saunders, and B. A. Korgel, "General shape control of colloidal CdS, CdSe, CdTe quantum rods and quantum rod heterostructures," *J. Phys. Chem. B.* **109**, 8538-8542 (2005).
 19. X. Chen, A. Nazzal, D. Goorskey, M. Xiao, Z. Adam Peng, and X. Peng, "Polarization spectroscopy of single CdSe quantum rods," *Phys. Rev. B: Condens. Matter* **64**, 2453041-2453044 (2001).
 20. J. R. Lakowicz, *Principles of fluorescence spectroscopy* (Kluwer Academic/Plenum, New York, 1999).
-

1. Introduction

In the past decade 2P excitation has been widely applied in a variety of materials to produce 3D refractive-index contrast due to its high spatial resolution to confine the light to 3D [1-7]. However a high 2P sensitivity and a large 2P absorption cross section are required to produce high precision photonic devices. In addition, not many organic dyes can introduce a localized polarization sensitivity which gives rise to the platform for light confinement in multi-dimensional in both spatial and polarization domains. Although it has been reported that azo dyes can be aligned under linearly polarized 2P illumination [8, 9], low 2P absorption efficiency remains them impractical in widespread applications. Semiconductor quantum rods (QRs) are particularly attractive because they are 2P excitable [10, 11] and have a broad spectral tunability over both the excitation and emission spectra [12, 13]. The 2P absorption cross section of QRs has been found to be $(20.9 \cdot 10^{-46} \text{ cm}^4 \cdot \text{s} \cdot \text{photon}^{-1})$ [14], 3 orders of magnitude higher than organic dyes, which makes them promising to be employed as 2P energy transfer (ET) donors in QR-dye assemblies. In particular, shaping nanoparticles into a rod form enables additional polarization-selective absorption and linearly polarized emission properties [15], which makes QRs perfectly suitable for 2P induced localized polarization control.

2. Materials

The principle of polarization refractive-index modulation we propose is based on ET from QRs to azo dye molecules as shown in Figs. 1(a) to 1(c). Dyes and QRs are randomly dispersed in the polymer matrix as shown in Fig. 1(a). ET can occur when dyes in the proximity of the Förster distance have their absorption band (red curves) overlapped with the emission band of QRs (blue curves). In this process, QRs pump weakly absorbing azo dye molecules, 5 orders of magnitude smaller than QRs, (2P absorption cross section on the order of $10^{-50} \text{ cm}^4 \cdot \text{s} \cdot \text{photon}^{-1}$) [16] when the illumination has a polarization parallel to the orientation of QRs (Fig. 1(b)). Consequently, the ET-driven isomerization of the azo dyes can re-orientate their optical axis towards the perpendicular direction of the illumination polarization, resulting in an anisotropic change in refractive index [9, 17]. When the illumination beam is perpendicularly polarized, QRs cannot be excited efficiently. Thus, neither can the ET-driven isomerization (Fig. 1(c)). Providing that the difference of the 2P excitation efficiency of rods between parallelly and perpendicularly polarized irradiation is large, the selective excitation between the different polarization angles enables the polarization modulation of the refractive-index change.

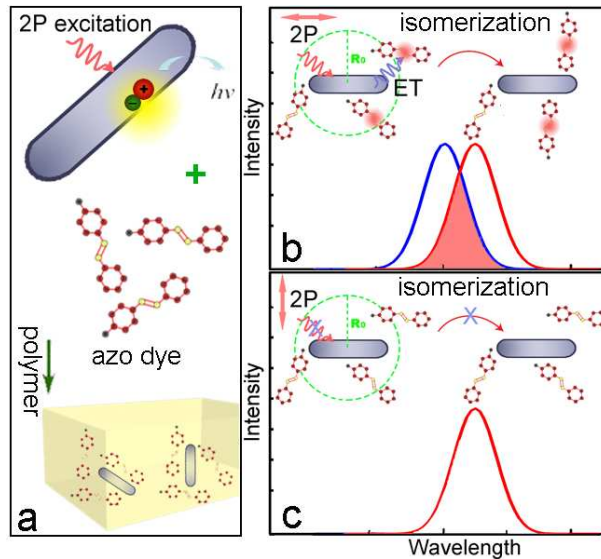


Fig. 1. Principle of polarization modulated energy transfer. (a) Fluorescent QRs and azo dyes are randomly dispersed in the polymer matrix. (b) When a laser beam is parallelly polarized to the orientation of QRs efficient 2P excitation and ET occur, which drives the re-orientation of azo dyes to the perpendicular direction to the laser polarization. (c) 2P excitation is shut off when the laser beam is perpendicularly polarized.

CdS rods were prepared following the well developed recipe [18]. The TEM image of as-prepared QRs is shown in Fig. 2(a) with an average size of 4.6 nm by 32 nm. The absorption and emission spectra of CdS rods in solution are shown in Fig. 2(b). The measured fluorescence (FL) quantum yield of CdS rods was 0.06 using 9,10-Diphenylanthracene as standard with known $\Phi_f = 0.95$. Single rods show a linearly polarized absorption behaviour under both single-photon excitation and 2P excitation [10, 15, 19]. A pronounced angular-dependent 2P excitation property has also been observed for our as-prepared rods on glass slide as shown in Fig. 2(c). It is seen that the angular dependence of excitation for both two emission spots (red and blue circles) is evidently clear and fits well with the curve of $\cos^4(\theta)$ (solid curves), which means QRs can be excited efficiently when the laser polarization is rotated parallel to the rod orientation, whereas the excitation is nearly shut off when the polarization is normal to this angle. The large contrast of the angular-selective excitation establishes the strength of polarization modulation of the consequent ET-driven refractive-index change.

First we demonstrated that local ET can indeed occur from QRs to azo dyes. Azo dye Disperse Red 1 (DR1) (Sigma Aldrich) was modified into 2-{ethyl-[4-(4-nitro-phenylazo)-phenyl]-amino}-ethyl ester (DR1-EH) to make it more soluble in the polystyrene (PS) matrix. The absorption band of DR1-EH, which gives sufficient spectral overlapping with the emission band of the QRs, is plotted in Fig. 2(b). The calculated Förster distance R_0 is 2.9 nm using the Förster formula [20]. CdS rods were dispersed in the PS matrix at a concentration of an average inter-particle distance of 86 nm for the given density of the polymer composition equal to 1 g/ml. A Ti:sapphire ultrashort pulsed laser beam of pulse width 100 fs (Spectra-Physics Tsunami) was employed as a 2P excitation source. The wavelength was specifically chosen at 720 nm to avoid the direct laser excitation of DR1-EH so that most irradiation energy is absorbed by QRs and transferred to dyes (see the absorption spectra in Fig. 2(b)). When the acceptors are far away from the donors, no ET occurs and strong FL emission of QRs is observed as illustrated in Fig. 3(a). The FL intensity of QRs is plotted as a function of the average inter-molecule distance between DR1-EH $\langle d_{\text{azo}} \rangle$ as shown in Fig. 3(b). The

images are shown in the inset. As we gradually increased the concentration of DR1-EH, which corresponds to the decrease in the inter-molecule distance between dyes, the FL intensity of QRs was reduced as a result of ET from QRs to DR1-EH. When the inter-molecule separation between DR1-EH is below 2.5 nm, the FL of QRs was quenched completely.

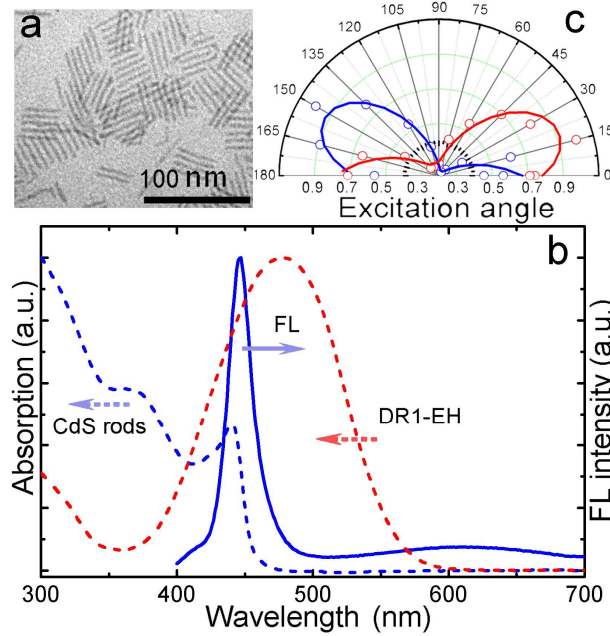


Fig. 2. (a). TEM images of as-prepared CdS rods. (b) Absorption and emission spectra of CdS rods as well as sufficient spectral overlapping with the absorption spectra of DR1-EH. (c) The angular-selective excitation of two emission spots of QRs prepared on the glass slide. The normalized FL intensity is plotted as a function of excitation polarization angles.

As schematic illustration in Fig. 3(a), when donors and acceptors are close in the proximity of R_0 azo dyes are excited as a result of ET occurrence. To observe the ET-driven isomerization-induced refractive-index change several bits were recorded in a sample doped with DR1-EH at a concentration of 9.1 wt% corresponding to an inter-molecule separation of 2.4 nm and differential interference contrast (DIC) microscopy was used to readout the refractive-index change of the written bits. QRs were diluted to an inter-particle separation of 104 nm to avoid aggregation. Assuming a homogeneous QRs distribution each rod consumes a volume of radius r . Within the volume of radius R_0 azo dyes are excited via energy transfer from QRs and the rest part is excited by direct laser excitation. The volume absorption cross section is given as $a = V \cdot \sigma_2$. With the given 2P absorption cross section of QRs is $20.9 \cdot 10^{-46} \text{ cm}^4 \cdot \text{s} \cdot \text{photon}^{-1}$ and the cross section of azo dye at excitation 720nm is approximately $5 \cdot 10^{-50} \text{ cm}^4 \cdot \text{s} \cdot \text{photon}^{-1}$ [16]. Special care is taken for surface capping which can give a reasonable homogeneous distribution $r=25\text{nm}$. The energy transfer induced excitation is given $a = \frac{4\pi R_0^3}{3} \sigma_2 = 2.2 \cdot 10^{-64} \text{ cm}^7 \cdot \text{s} \cdot \text{photon}^{-1}$. Whereas the background absorption from the 2P excitation of dye molecules is given $a_{\text{dye}} = \frac{4\pi r^3}{3} \sigma_2 = 1 \cdot 10^{-66} \text{ cm}^7 \cdot \text{s} \cdot \text{photon}^{-1}$, which is two orders of magnitude smaller than

energy transfer induced excitation. In our experiment condition to avoid aggregation we decreased concentration of QRs with $r=52\text{nm}$. The energy transfer induced excitation is still one order of magnitude larger than 2P excitation of dyes where $a = \frac{4\pi r^3}{3} \sigma_2 = 5.3 \cdot 10^{-65} \text{ cm}^7 \cdot \text{s} \cdot \text{photon}^{-1}$. As a result contribution of 2P excitation of dye molecules to the refractive-index change is nearly negligible.

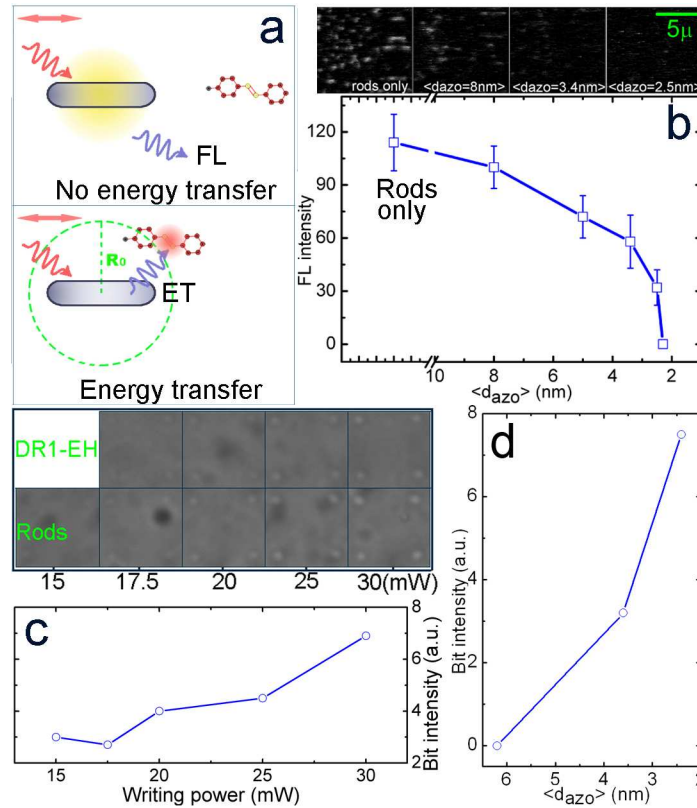


Fig. 3. (a). Schematic illustration when donors are far away from acceptors, no ET occurs and FL is emitted from QRs. If donors and acceptors are close in the proximity of Förster distance, azo dyes are excited by ET. (b). FL intensity of the QR-dispersed PS sample is plotted as a function of the inter-molecule separation of DR1-EH. The inset is the FL images for different azo dye concentrations. (c). Readout bit intensity of pure ET-driven isomerization induced recording is plotted as a function of the writing power. DIC images are shown in the inset. (d). The readout bit intensity of pure ET-driven isomerization induced recording at 30 mW in samples blended with azo dye of different concentrations.

The readout bit intensity of pure ET-driven isomerization induced recording is simply given by subtracting the background recording of DR1-EH itself and plotted as a function of the writing power, shown in Fig. 3(c). The DIC images are shown in the top inset. Increase in the writing power leads to significant increase of the readout intensity due to complete transfer of QRs absorbed 2P energy to surrounding azo dyes. Reducing the concentration of azo dyes leads to incomplete energy transfer and decreases the recording efficiency. This is observed in Fig. 3(d). The readout bit intensity of pure ET-driven isomerization induced recording at 30 mW is plotted as a function of mean separation between azo dyes. It is evident that the readout intensity of energy-transfer induced recording is gradually increased as the progressive increase of energy transfer efficiency by reducing of $\langle d_{\text{azo}} \rangle$.

3. Results

ET-driven isomerization induced by angular selective excitation of QRs introduces polarization sensitivity which is characterized by pump-probe experiment. A linearly polarized white light source with central wavelength at 520 nm and a full width at half maximum of 10 nm was employed as a probe beam. The transmitted probe beam intensity was monitored by a CCD (PIXIS 100, ACTON). Spincoated samples of thickness of 4 μm with an inter-molecule separation of 2.4 nm between DR1-EH and the inter-particle distance of 104 nm between rods were prepared. Generally *trans* molecules have a larger extinction coefficient compared with *cis* molecules. They are selectively photobleached and re-orientated during the isomerization process leading to angular hole burning absorption [8]. The absorption decrease is much stronger when the laser polarization is parallel to the probe beam than it is normal to the probe. Figure 4(a) shows the pure ET-driven absorbance evolution after baselined to controlled sample dispersed DR1-EH itself to subtract the background recording. The absorbance decrease here is due to pure ET-driven isomerization induced angular hole burning of *trans* molecules. The early isomerization rates in the first 40 seconds were fitted with linear dependence. It is clear to see that the rate of the absorbance change in the parallel direction is significantly faster than that in the perpendicular direction where the difference is over 5 times. This is primarily attributed to the strength of the angular selective excitation property of QRs where the excitation is nearly shut off in the perpendicular direction.

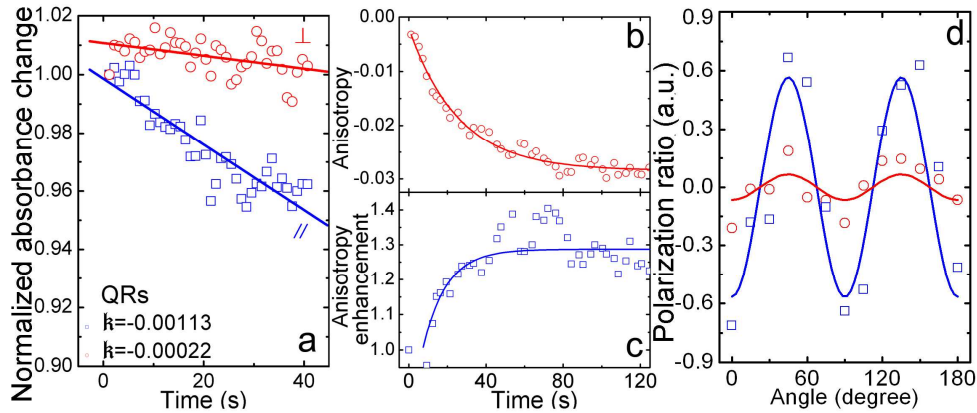


Fig. 4. (a). Pure ET-driven angular hole burning absorption in QR-sensitized sample after baselined to DR1-EH to subtract the background. The irradiance intensity is $15 \text{ GW} / \text{cm}^2$. Blue squares and red circles are data when the beam is parallelly and perpendicularly polarized to the probe beam, respectively. Solid lines are fitting with a linear dependence to give early isomerization rates. (b) Anisotropy evolution of the QR-sensitized sample under linearly polarized illumination. The solid line is the guide for eyes. (c) Anisotropy enhancement of QR-sensitized sample compared to the QD-sensitized sample is plotted as a function of time. The solid line is the guide for eyes. (d) Plot of ET-preserved polarization ratio of recorded bits as a function of reading polarization angle after baseline the bit intensity at each reading polarization angle with DR1-EH itself. Red circles and blue squares are data from QDs- and QRs-sensitized sample respectively. Solid curves are fitting with $\cos(4\theta)$.

The large difference of the isomerization rates in parallel and perpendicular directions builds up the anisotropy as well as the localized polarization sensitivity. Figure 4(b) shows ET-driven anisotropy evolution $A(t)$ [8] in the QR-sensitized sample. The anisotropy increases exponentially and reaches the maximum within 120 s and slowly reverses after that. The pronounced polarization-selective excitation property of QRs creates a maximum anisotropy of approximately -0.03 which is abundant to enable the following localized

polarization modulated photonic applications. For a comparison a CdS quantum dot (QD)-sensitized sample was prepared at the same concentration. As spherical QDs have no angular-selective excitation property random re-orientation is expected. The residual polarization sensitivity is mainly attributed to weak background recording by direct excitation of dyes. Figure 4(c) shows the plot of the anisotropy enhancement defined as $R(t) = A_{rods}(t)/A_{dots}(t)$, where $A_{rods}(t)$ and $A_{dots}(t)$ are anisotropy in QR- and QD-sensitized samples, respectively. The anisotropy enhancement from Fig. 4(c) reveals that the polarization sensitivity can be preserved during QR-driven ET process. This ET-preserved polarization has been confirmed by the polarization readout of several bits recorded by a parallelly-polarized beam. The polarization sensitivity of recorded bits was readout between two orthogonal polarizers [9]. After baseline the bit intensity at each reading polarization angle respect to the controlled sample, the polarization ratio of pure ET-driven isomerization induced recording is plotted as a function of reading polarization angles in Fig. 4(d). It can be seen that the pronounced polarization sensitivity is preserved in the QR-driven ET process whereas the polarization in QDs sensitized sample is negligible.

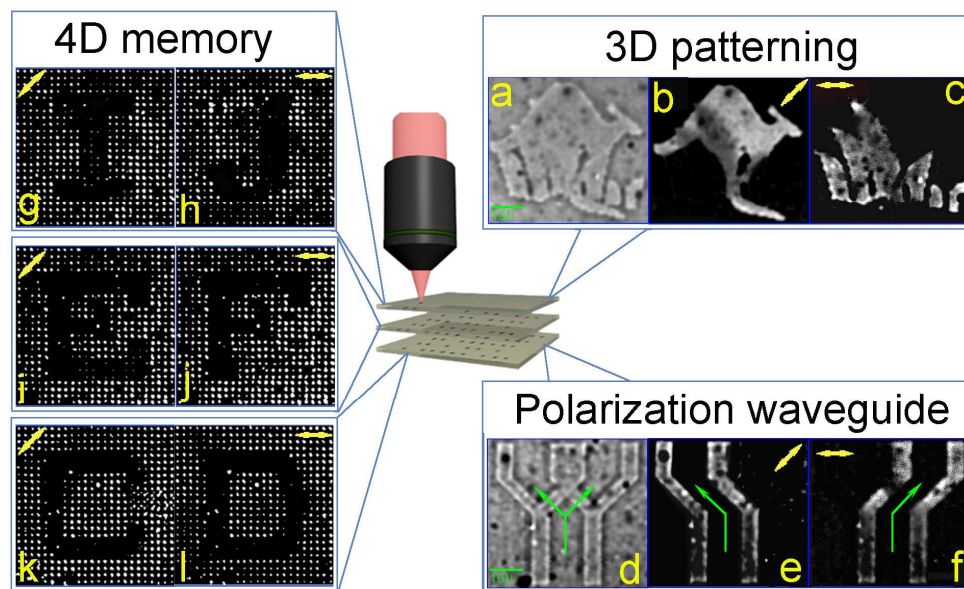


Fig. 5. Photonic applications of localized polarization control. (a) DIC images of polarization multiplexed patternings. Top-view images of distinct patterns are retrieved by rotating the polarization direction of the reading beam at 45 (b) and 0 (c) degrees, respectively. (d) DIC images of polarization controlled waveguide fabrication. Top-view images of upper and lower arms are readout at a polarization angle of 45 (e) and 0 (f) degrees, respectively. g-l are the demonstration of polarization-multiplexed 4D optical memory. Letters I/J (g/h), E/F (i/j) and C/D (k/l) were recorded in the first, second and third layers, respectively, in the polarization direction of 0 and 45 degrees and retrieved back using corresponding polarized reading beams.

The localized polarization sensitivity offers an additional dimension to manipulate the beam in the polarization domain, which holds a great potential of multi-dimensional photonic applications. Figures. 5(a) to 5(f) demonstrate polarization multiplexed 3D patterning and fabrication of waveguides. Patterns of a kangaroo and the Sydney Opera House have been multiplexed in the same position when the polarization direction of the writing beam is orientated at 0 and 45 degrees, respectively. Refractive-index variation is shown in the DIC readout image in Fig. 5(a). The patterned images can be retrieved distinctly using reading beam of a polarization angle at 45 and 0 degrees, respectively, shown in Figs. 5(b) and 5(c). Similarly, a Y-shape waveguide channel was fabricated with the support region of upper and

lower arms at 0 and 45 degrees of the reading polarization direction, respectively. This polarization-multiplexed waveguide could be used to split and guide differently polarized beams. The principle can also be applied in the polarization-encoded four-dimensional (4D) optical data storage as shown in Figs. 5(g) to 5(l). Letters I/J, E/F and C/D were encoded at the 0 and 45 degrees of the writing polarization direction in the first, second and third layers, respectively. Data can be retrieved out using a corresponding polarized reading beam. The principle of the 3D localized polarization control in the newly developed QR-dispersed polymer can also be used to manipulate photons in four dimensions in a 3D photonic crystals [1].

4. Conclusion

In conclusion, we have incorporated CdS QRs with vast 2P absorption cross-sections into azo dye dispersed polymer composites via 2P energy transfer. Enhanced recording efficiency and polarization preserved energy transfer from QRs to surrounding azo dyes have been observed, which facilitates the re-orientation of azo dye optical axis to the perpendicular direction to the polarization of writing beams. Therefore anisotropic refractive-index variation has been achieved. Application of this new material into polarization encoded four-dimensional optical data storage, patterning and polarization-controlled waveguide fabrication has been successfully demonstrated.

Acknowledgments

The authors acknowledge the support from the Australian Research Council and thank Dr. Joel Van Embden (Swinburne University of Technology) for fruitful discussion. This research has been supported by the Australian Research Council.